Journal of Power Sources 570 (2023) 233063

Contents lists available at ScienceDirect

Journal of Power Sources

journal homepage: www.elsevier.com/locate/jpowsour

A new shape-conformable battery concept: The 3D printed injectable battery filled with semi-solid electrodes

Mario Borlaf [a,b,**,1], Rodrigo Moreno [c], Edgar Ventosa [a,b,*]

[a] Universidad de Burgos, Facultad de Ciencias, Dpto. Química Analítica, Plaza de Misael Bañuelos S/N, 09001, Burgos, Spain
[b] International Research Center in Critical Raw Materials for Advanced Industrial Technologies (ICCRAM), Edificio I+D+I/CIBA, Plaza de Misael Bañuelos S/N, 09001, Burgos, Spain
[c] Instituto de Cerámica y Vidrio, Consejo Superior de Investigaciones Científicas (ICV-CSIC), Kelsen 5, 28049, Madrid, Spain

HIGHLIGHTS

- Semi-solid electrodes and 3D printing is combined to fabricate batteries.
- The proof-of-concept for a new type of shape-conformable batteries is demonstrated.
- A UBU-shaped battery is fabricated based on MnO_2 and Zn metal.
- Acceptable cycle stability (0.45% h^{-1}) are achieved.
- MnO_2-based semi-solid electrodes deliver >150 mAh $g_{MnO_2}^{-1}$.

GRAPHICAL ABSTRACT

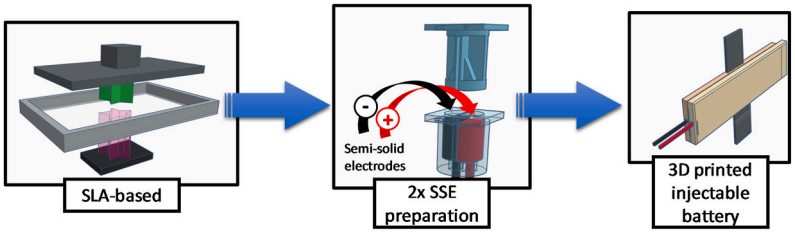

ARTICLE INFO

Keywords:
Additive manufacturing
Shape-conformable batteries
Semi-solid electrodes
Zn–MnO_2 rechargeable batteries

ABSTRACT

Shape-conformable batteries are of high interest for a variety of portable electronics. In this work, a new manufacturing concept for cost-effective shape-conformable batteries based on the combination of additive manufacturing (AM) technology and semi-solid electrodes (SSEs) is proposed. The manufacturing process consists in two steps. Firstly, the electrochemical cell is printed by stereolithography-based technique (SLA) and subsequently assembled. In a second step, flowable SSEs are injected into the cells by a double injection mechanism to introduce both SSEs in parallel. While syringe outlets, cell inlets and shape of the cell are found to play an important role in the injection process, formulation of the SSEs are observed to influence the rheological and electrochemical properties. For the proof of concept, a battery having the shape of the logo of our university is fabricated using Zn-based and MnO_2-based SSEs achieving high utilization rate (>150 mAh $g_{MnO_2}^{-1}$) and acceptable cycle stability (0.45% h^{-1}) and thus showing the feasibility of the proposed shape-conformable injectable battery. The manufacturing process is finally extended to other battery chemistries leading to improved cycling stability and confirming the versatility of the manufacturing concept.

* Corresponding author. Universidad de Burgos, Facultad de Ciencias, Dpto. Química Analítica, Plaza de Misael Bañuelos S/N, 09001, Burgos, Spain.
** Corresponding author. Universidad de Burgos, Facultad de Ciencias, Dpto. Química Analítica, Plaza de Misael Bañuelos S/N, 09001, Burgos, Spain.
E-mail addresses: mario.borlaf@uam.es (M. Borlaf), eventosa@ubu.es (E. Ventosa).
[1] Present address: Universidad Autónoma de Madrid, Facultad de Ciencias, Dpto. Química Inorgánica, Francisco Tomás y Valiente 7, 28049 Madrid, Spain.

https://doi.org/10.1016/j.jpowsour.2023.233063
Received 23 November 2022; Received in revised form 22 March 2023; Accepted 5 April 2023
Available online 12 April 2023

1. Introduction

Batteries have become key elements in our daily lives, being used in many applications ranging from buffering energy produced from intermittent renewable sources to electric vehicles. Usually, batteries are the power sources of electronics and they are integrated into them, especially for portable ones (phones, tablets, smartwatches, etc.). Therefore, having an easily integrable battery would be a great asset. The fabrication of a battery acting as frame of an electrochromic sunglasses as well as powering it is a good example of the potential benefits of shape-conformable batteries for the industry of portable electronics and other fields as aviation [1–5]. Therefore, the scientific community is devoting great efforts in exploring conceptually new approaches to develop battery technologies that enable simple and cost-effective fabrication of shape-conformable batteries with complex architectures to directly integrate them in portable devices.

In this context, conventional manufacturing process can be considered as a *top-down* approach. First, energy-storing materials are fixed on current collectors using a roll-to-roll process. Large sheets coated with energy-storing materials are then cut into smaller pieces, and finally batteries are assembled. This top-down approach is cost-efficient for batteries of relatively large dimensions, but it restrains the capability of fabricating shape-conformable and complex architectures, especially of small dimensions. On the other hand, additive manufacturing (AM) is a bottom-up approach that enables manufacturing of specific complex architectures [1,2,6]. Thus, AM of batteries is attracting much attention since this approach is perceived as a key enabler for several emerging fields. Although great progress has been made in 3-D printing of batteries, there are a series of major challenges that AM of batteries faces. Pang et al. [7] summarized the main challenges for lithography based 3-D printing, template-assisted electrodeposition-based 3-D printing, inkjet printing, direct ink writing, fused deposition modeling (FDM), and aerosol jet printing: I) There are only a few printable materials, especially active materials, that can be used as inks for 3-D printing batteries. II) The porous structures introduced in 3-D printing fabrication processes lead to poorer mechanical properties and weakly bonded interfaces between layers. III) High-temperature post-processing is typically required for 3-D printing fabrication of batteries, resulting in low-rate capabilities, and increasing the costs. IV) Water vapor and oxygen in the air have significant effects on the performance of active electrode and electrolyte materials (this issue is common for conventional Li-ion batteries). V) The compatibility of the inks for each component to be printed sequentially and successfully remains a big challenge. As a result, blooming of AM of batteries will require either i) several breakthroughs to tackle each major challenge at a time, or ii) a freshly new conceptual approach based on 3-D printing.

In a conventional approach, active materials are fixed onto the current collector for non-flow batteries regardless traditional manufacturing or AM is used for their fabrication. However, the disruptive work from Duduta et al. [8] that proposed a new type of electrode based on traditional intercalation materials untapped a new direction in batteries: the semi-solid electrodes (SSEs). The main feature of SSEs is the lack of binder so that their flowability, among other characteristics, can be tuned by changing the ratio between active material, carbon additive and electrolyte. Originally, these new types of electrodes were employed to boost energy density for redox flow batteries [9–11], but afterwards other features, e.g. enhanced transport of ions, were exploited for non-flow batteries [12]. Recently our group explored the benefits of SSEs with intermediate rheological properties, so-called pseudo-flowable SSEs, to facilitate the recyclability of non-flow batteries since electrodes can be easily recovered once the end of life of the battery is reached, and the entire electrochemical cell can be reused (reducing costs) [13–15]. The emerging field of SSEs opens new possibilities for new battery concepts due to their unique properties.

In this work, another unique feature of SSEs, i.e., its plasticity, is exploited to propose a new type of shape-conformable battery technology. In short, 3D printed injectable batteries with complex shapes are fabricated by the combination of AM and SSEs technologies. Using a stereolithography (SLA) – based 3D printer, the electrochemical cell, and the injection parts (syringe and other pieces) are first produced. Once the cells are assembled, aqueous Zn-based and MnO_2-based SSEs are prepared and injected into the cells demonstrating the possibility of fabricating shape-conformable injectable batteries. The system Zn–MnO_2 is chosen as a case of study because it is based on aqueous electrolyte that facilitates the demonstration and both are abundant materials that are commercially available for accelerated development. Preliminarily results with other battery chemistries confirm the versatility of the proposed battery manufacturing concept.

2. Experimental

2.1. Materials and reagents

SSEs were prepared by using Zn powder (99.9%, 100 mesh, Alfa Aesar, USA) and MnO_2 (courtesy of CEGASA, Spain) as active materials. An electroconductive carbon black powder (KetjenBlack EC-600JD, Nanografi, Turkey) was used as carbon additive to enhance the electrical conductivity. $Zn_2SO_4{\cdot}7H_2O$ (98%, Alfa Aesar) and $MnSO_4$ (99%, Alfa Aesar) were used to prepare the electrolyte in the following concentrations: Zn^{2+} (2 M) + Mn^{2+} (0.1 M) dissolved in water.

For the battery, expanded graphite (bipolar plate Sigracell TF6, SGL Carbon, Germany) was used as current collectors and CELGARD 3501 (CELGARD, USA) as separator. The current collectors of the complex shape batteries were cut with a cutting machine Silhouette Cameo 4 (Silhouette, USA).

2.2. Electrochemical cells fabrication and assembling

The battery half-cells were fabricated using an Ultraviolet (UV) Liquid Cristal Display (LCD) – based stereolithography (SLA) 3D printer Photon Mono SE (Anycubic, China) and a commercial clear resin (Anycubic, China). After the cleaning procedure (with 70% isopropanol solution), the current collectors were introduced into each half-cell and then, the separator was put between both, leaving two cavities that will be filled in a subsequent step with the SSEs (Fig. 1). In all batteries, the height of the cavities, i.e., the thickness of the SSEs, was 1 mm. For the simple shape batteries, an active area of 50×10 mm^2 was used (total dimensions of the full battery are 58×18×6 mm^3).

The injection procedure was carried out by using our own 3D printed syringes and connections to inject both SSEs at the same time (see section 3.2).

2.3. Semi-solid electrodes preparation

The SSEs were prepared by dispersing the active material and the carbon into the electrolyte at different solids loading, using the Ultraturrax (IKA, Germany) mixer. The materials and the electrolyte were put into a 20 mL commercial syringe (B|Braun Injekt, Germany) and then, they were mixed. When the SSE was formed, it was transferred into the double injection 3D printed syringe. The following electrode formulations were used: MnO_2 SSEs: 1 g of MnO_2 and 0.375 g of carbon were dispersed into the Zn^{2+} (2 M) + Mn^{2+} (0.1 M) aqueous electrolyte (different volumes were tested); Zn SSEs: 1 or 2 g of Zn and 0.420 g of carbon were dispersed into the Zn^{2+} (2 M) + Mn^{2+} (0.1 M) aqueous electrolyte (different volumes were tested).

2.4. Characterisation of semi-solid electrodes and batteries

Rheological measurements of the SSEs were performed by using a rotational rheometer (RS50, Thermo Scientific Haake, Germany) with a plate-plate configuration and a gap of 1 mm. Flow curves were measured with an increase of the shear rate from 1 to 65 s^{-1} in 120 s, a plateau at

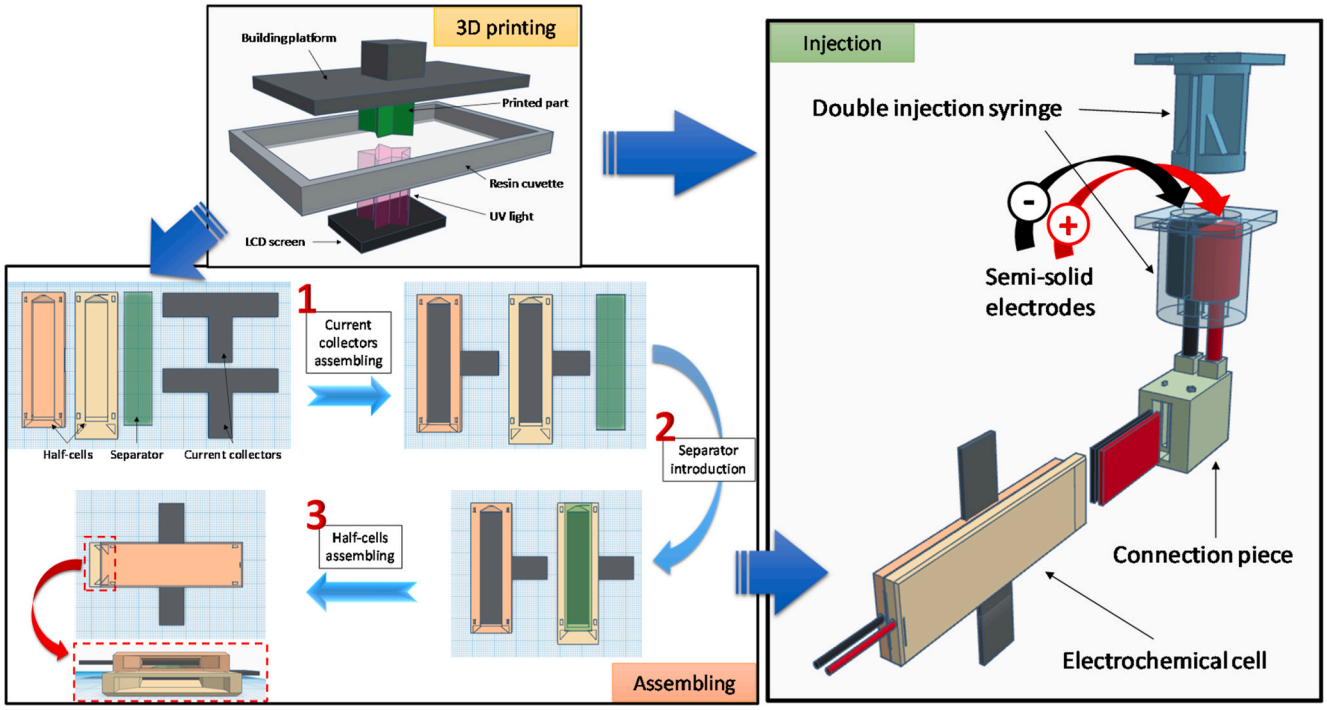

Fig. 1. Description of the fabrication process of a 3D printed injectable battery. 3D printing (CAD model design and 3D printing of the pieces), assembling (current collector, separator and half-cells assembling, a zoom of the inlet is also shown) and injection (SSEs preparation, transfer to the 3D printed syringe, connection with the empty electrochemical cell and injection) steps.

65 s^{-1} for 60 s, and a decrease to 1 s^{-1} in 120 s.

Galvanostatic charge-discharge measurements were carried out by using a cycler (NEWARE, China) at a current density of 2 $mAcm^{-2}$ and a voltage ranging between 0.7 and 1.7 V.

3. Results and discussion

3.1. A new shape-conformable battery concept

The shape-conformable injectable battery possesses a disruptive approach for the fabrication of energy storage systems in terms of design and degrees of freedom. The innovative nature of our approach relies on two emerging technologies: (1) the additive manufacturing (design and fabrication parameters) and (2) the SSEs (viscosity, flowability and electrochemistry).

Fig. 1 shows a summary of the fabrication process of 3D printed injectable batteries. In a first step, the computer-aided design (CAD) models of the half-cells, syringes and connection pieces are created and sent to the 3D printer. Once the pieces are printed and cleaned, the current collectors are introduced into the half-cells (1), followed by the placement of the separator on the top of one half-cell (2) and they are subsequently assembled (3). The full cell without electrodes has empty cavities to be thoroughly filled with SSEs. In parallel, the SSEs are prepared and transferred to the double syringe, which is connected to the auxiliary piece that joints the electrochemical cell and the syringe. After that, the injection process is initiated until an excess of SSEs goes out through the outlet of the battery cell.

This methodology allows the fabrication of batteries with high versatility from different points of view: I) Cell design: it can be easily modulated thus allowing the manufacture of batteries with simple or complex shapes. Additionally, it is possible to modulate the capacity of the cavities for the injection of the SSEs. II) Injection process: it should be configured to obtain a fully injected battery. The connector that joins the injector and the cells can be designed to optimise injection performance. III) SSEs formulation: the composition of the SSEs should be adapted to each cell and injection mechanism to achieve a fully injected battery with the desired electrochemical performance as the formulation influences on both the rheological and electrochemical properties of the resulting SSEs.

3.2. Design of the electrochemical cell and injection system

Initially, rectangular shapes were used to evaluate the printing, assembling and injection processes by analysing the electrochemical performance of the resulting batteries. According to the assembling process shown in Fig. 1 (5 cm^2 of active area), three main issues must be considered for each half-cell: 1) the cavity for the current collector, 2) the cavity for the SSE, and 3) the inlet and outlet for the injection process. The latter deserves special attention since it plays an important role in the filling of the cells, in the proper contact between the SSE and the current collector, and between the two SSEs through the separator. Based on that, three different inlets were designed (Fig. 2). The first type of studied inlet (Fig. 2A) is based on a simple strategy that consists in the injection of the SSEs with the same dimensions as that of the cavity left for such purpose (section of 10 × 1 mm^2). The second type of studied inlet (Fig. 2B) consists in an injection with the same dimensions as that of the cavity but, in that case, there is a change of the SSE shape from cylindrical to rectangular in a perpendicular way. This strategy leads to a compression of the SSE before being introduced into the cavity of the electrochemical cell. The third type of studied inlet (Fig. 2C) consists in a progressive reduction of the SSE rectangular shape from 15x2 to 10 × 2 mm^2. In that case, the strategy is to ensure two different compressive processes in width and height (thickness) of the SSE. Moreover, an additional piece was necessary, which is referred to as connector (Fig. 2C).

In all cases, a double injection syringe was used to fill the battery with both SSEs at the same time (Fig. 2C), and only the outlet of the syringe was modified. For the first case, an outlet with rectangular shape was designed to be inserted into the inlet of the electrochemical cell, (Fig. 2A). Thus, the shape of SSE is already limited by the outlet of the

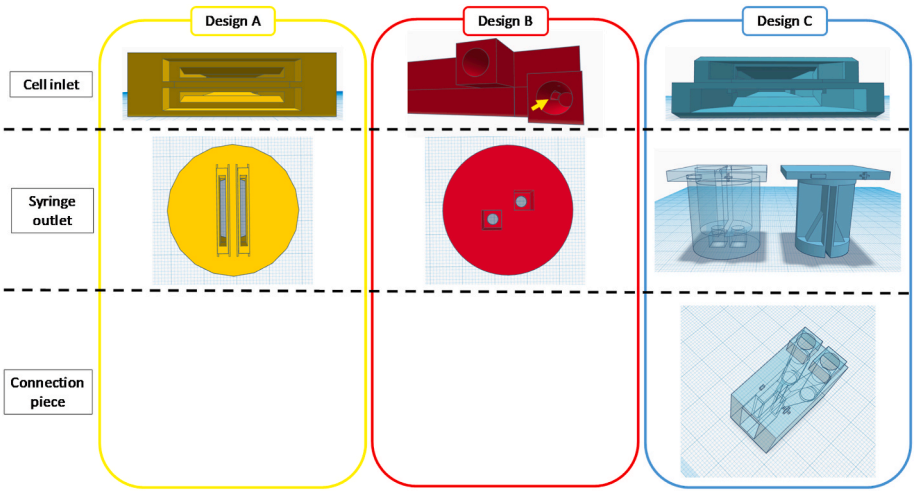

Fig. 2. Cell inlets and syringe outlets of all double injection system and connection piece for design C.

syringe. For the second one (Fig. 2B), the syringe had a square main section of 3 mm, shaping into a cylindrical outlet of 2 mm. In this way, the cylindrical outlet acts as a section reduction leading to a compression in the SSE. In the third type (Fig. 2C), the design also aims at inducing a compression in the SSE during the injection, but in that case, a progressive compression occurs via a 3-piece system. The first element is the syringe outlet that shapes the SSE into a cylindrical geometry of 5 mm diameter. Outlet of the syringe fits into a connection piece, which modifies the shape of the SSE progressively from the 5 mm cylindrical shape to a 15 × 2 mm^2 rectangular one in a perpendicular way. At the end of the connector there is an outlet where the electrochemical cell is inserted, which completes the shaping of the SSE into the desired shape.

For the optimization of the injection process, Zn–MnO_2 batteries were used. SSEs based on 1 g of active material, 6 mL of electrolyte ($ZnSO_4$ 2 M + $MnSO_4$ 0.1 M) and 0.420 or 0.375 g of carbon for Zn or MnO_2 SSEs, respectively, were injected into batteries with an active area of 5 cm^2 and 1 mm of SSE thickness. The initial capacities of the batteries were 0.20, 0.59 and 0.94 $mAhcm^{-2}$ for the systems A, B and C, respectively. A theoretical value of 3.43 $mAhcm^{-2}$ was estimated considering a specific capacity of 220 mAh $g^{-1}_{MnO_2}$, a concentration of active material in the SSE (1 g in 6.0 mL), and a volume of SSE in the cell (0.5 cm^3). Although the three values are lower than the expected ones, a general conclusion is drawn: the system C led to significantly improved performances, which is likely associated with the compaction of the SSEs for this injection system. This should be related with the removal of the air trapped between particles during the SSEs preparation, which enhances the contact between them improving the electrical conductivity. Considering all aspects, the system C was selected for the injection process, using the same design for the fabrication of complex-shape batteries.

3.3. Tuning of the properties of SSEs

Fig. 3 shows the first discharge capacity as a function of the electrolyte volume for both SSEs for constant amount of active material and carbon additive (see voltage profiles in Fig. S1 and capacity values in Table S1). From battery number 1 to number 4, the progressive decrease in the volume of the electrolyte from 6.0 to 4.5 mL for both SSEs led to the progressive increase in capacity of the battery from 0.94 up to 2.84 $mAhcm^{-2}$. Further decrease in electrolyte volume down to 4.0 mL resulted in highly dense SSEs that were not possible to inject into the battery. Because of that and keeping constant the electrolyte volume of MnO_2-SSE at 4.5 mL, the batteries number 5 and number 6 were prepared by increasing only the electrolyte volume of Zn-SSE from 4.5 mL (battery 4) to 6.0 mL (battery 5) and to 7.5 mL (battery 6). The increase

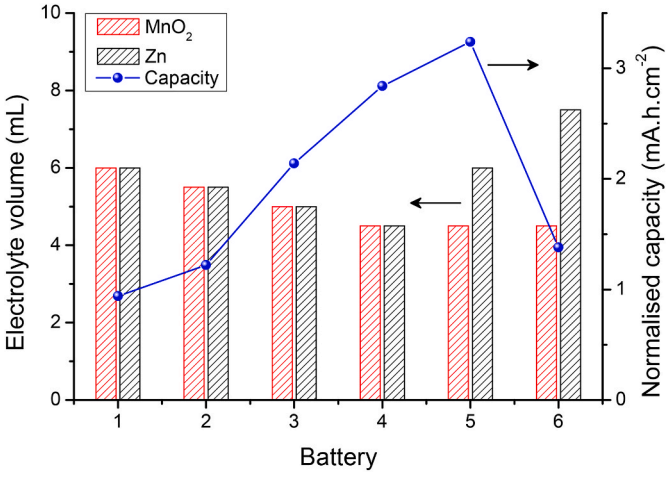

Fig. 3. Evolution of normalised capacity as a function of the SSEs electrolyte volume. MnO_2-SSE: 1 g MnO_2 and 0.375 g C. Zn-SSE: 1 g Zn and 0.420 g C.

in electrolyte volume from 4.5 mL to 6.0 mL led to an increase in the capacity up to 3.24 $mAhcm^{-2}$. However, further increase in volume to 7.5 mL resulted in a drop in capacity down to 1.38 $mAhcm^{-2}$. While the electrical contact is expected to worsen as the volume of electrolyte increases (concentration of carbon particle decreases), other factors must be considered to explain the trend. Likely, the unexpected improvement in capacity is related to the rheology of the Zn-SSE having 6.0 mL of electrolyte that may facilitate the simultaneous injections of Zn-SSE and MnO_2-SSE (see section 3.4).

The SSE formulation not only affects the electrochemical properties, but also the rheological behaviour, which is a key parameter for complex-shape injectable batteries [16]. For such purpose, six pieces were designed and fabricated to evaluate the injection process through simple injection tests (Fig. S2). The shape of the pieces was varied starting from a straight line and ending with a zig-zag configuration using an acute angle of up to 30°. Fig. 4 shows the photograph of the injection tests after being injected using different formulations (different electrolyte volumes) of Mn-SSEs. This simple injection test illustrates graphically the ability of the three SSEs to fill complex-shape cavities in the following order: 5.5 mL > 5.0 mL > 4.5 mL. These results are in good agreement with the viscosity curves shown in Fig. 5 and the values presented in Table S2, showing the importance of the SSE formulation in its rheological properties. Comparing both SSEs prepared with 6.0 mL of electrolyte, a difference of approximately one order of magnitude in the

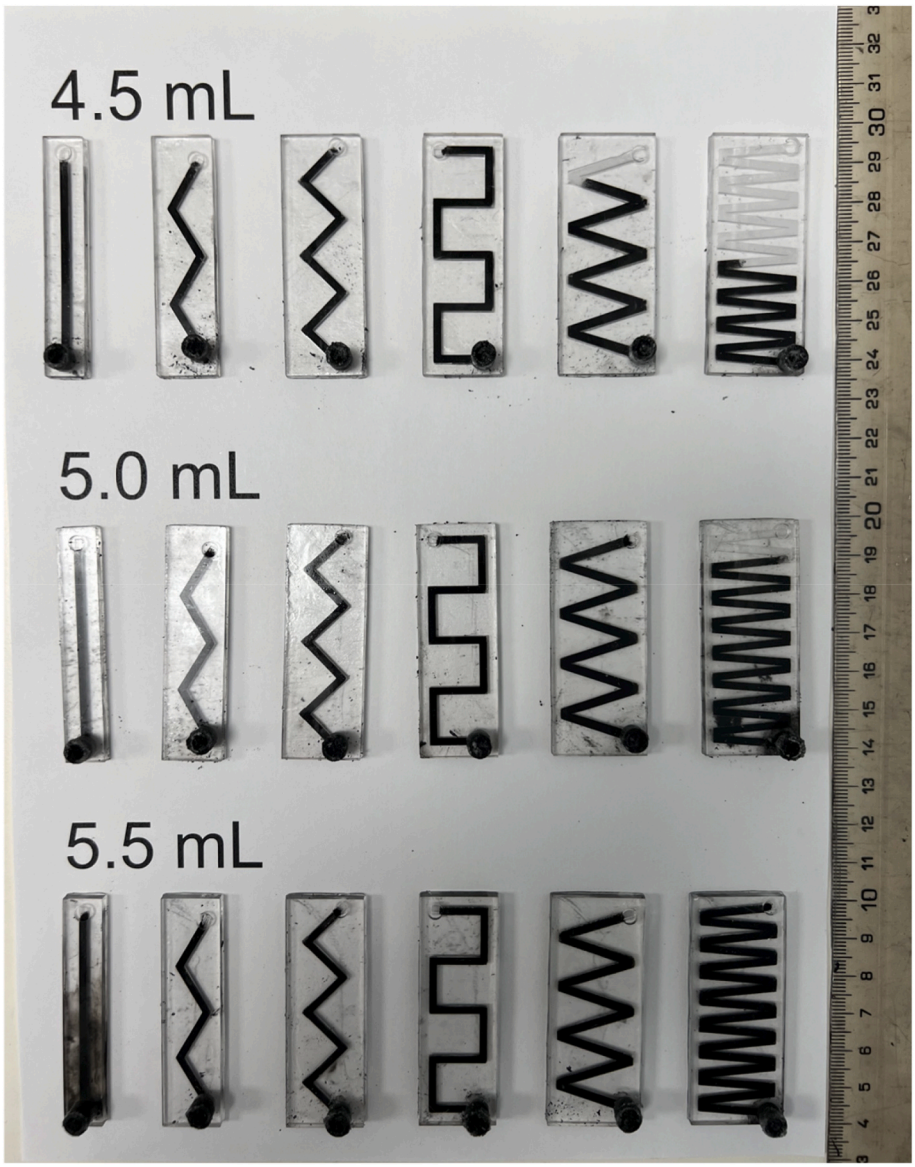

Fig. 4. Picture of the injection tests with the Mn-SSE (1 g MnO_2 and 0.375 g carbon) prepared with different electrolyte volume.

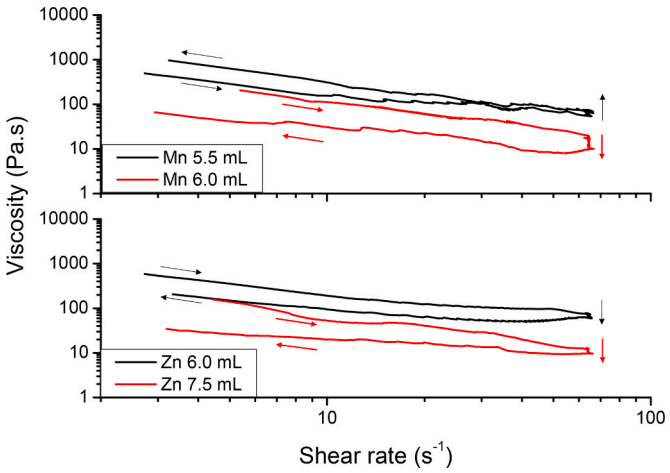

Fig. 5. Viscosity curves of different SSEs as a function of the shear rate. The content of MnO_2 (1 g) and carbon (0.375 g) for MnO_2-SSEs as well as the content of Zn (1 g) and carbon (0.420 g) for Zn-SSEs were kept constant.

viscosity values is observed. This is also related with the observation made at the end of the previous section, where an increase in the battery capacity was detected when the electrolyte volume of the Zn-SSE increased from 4.5 to 6.0 mL. The surface chemistry of the MnO_2 and Zn particles affects to the interaction with the other SSE components (carbon particles, solvated ions, and solvent molecules), affecting to the flowability of the SSEs and, for instance, to the injection and compaction processes. Note that rheological properties of the SSEs prepared with lower electrolyte volumes (below 5.5 mL) could not be measured because they blocked the torque of the rheometer, indicating that the viscosity was above 1.000 Pa. This explains the difficulties for SSEs having 5.0 and 4.5 mL to be successfully injected in the injection tests shown in Fig. 4. Moreover, these high viscosity values help to avoid sedimentation phenomenon, as desired to improve the performance of the proposed batteries. Analysing the viscosity curves, a decrease of 0.5 mL of electrolyte volume generates an increase in the viscosity from 203 to 712 Pa s (measured at 5 s^{-1}). When the electrolyte volume is decreased to 4.5 mL, the increase in the viscosity will be greater (measurements could not be performed because of torque blocking), making the sedimentation process minimal for a long time. To visualise the effect of the high viscosity to the readers, those SSEs are paste-like and can

be easily extrudable, keeping the desired shape without deformation for long time. All measured SSEs exhibited a shear thinning and thixotropic behaviour except the Mn-SSE prepared with 5.5 mL of electrolyte. The latter revealed an anti-thixotropic (rheopectic) phenomenon, although the area enclosed in the hysteresis cycle is lower, so that the injection of this SSE in the test piece with the highest complexity was allowed. While all tested SSEs were successfully injected for simple geometries as those used for the characterisation of the electrochemical properties, the injection tests shown in Fig. 4 predicts high difficulties for using certain SSEs in a complex-shape battery cells, e.g., Mn-SSEs using 4.5 mL electrolyte. The main reason is because of the rheopectic (anti-thixotropic) behaviour: a fluid becomes more viscous when a constant deformation, agitation, or other phenomenon is applied on it. Nevertheless, the injection process is not only influenced by the angle, but also by other parameters of the cell design, e.g., the length and section of the cavity. Fortunately, AM provides the versatility to propose strategies to implement viscous SSEs in complex-shape battery cells. For example, the introduction of a second injection inlet in the cell would shorten the distance that the SSE should cover. In that case, it would be possible to find an equilibrium between the rheological and the electrochemical properties of the SSEs without significantly sacrificing the shape of the cell.

3.4. Electrochemical characterisation of simple-shape batteries

Zn–MnO_2 batteries with an active area of 5 cm^2 (5×1 cm^2) were used to evaluate the electrochemical properties of SSEs. Based on the results shown in previous sections, three batteries were investigated using the following SSEs (1 g MnO_2 and 0.375 g carbon or 1 g Zn and 0.420 g carbon): (1) Mn-6.0 mL and Zn-6.0 mL (Mn60Zn60), (5) Mn-4.5 mL and Zn-6.0 mL (Mn45Zn60) and (6) Mn-4.5 mL and Zn-7.5 mL (Mn45Zn75), where Zn or Mn indicates the Zn or MnO_2 SSE and the number is the electrolyte volume used for their preparation. In all of them, the open circuit voltage (OCV) of each as-prepared battery was between 1.55 and 1.60 V. Fig. 6A shows the voltage-capacity profiles of the second cycle for the three batteries. In all cases, the two characteristic plateaus of the Zn–MnO_2 batteries associated to the two-phase reaction are well observed [17], although it is clearer in the battery 5 (Mn45Zn60), in which the highest capacity was obtained. Fig. 6B and C shows the coulombic efficiency and the evaluation of the areal capacity upon cycling for the three batteries. Overall, battery 5 (Mn45Zn60) delivered the best electrochemical performances which is attributed to better electrical contact for these SSEs due to the lower amount of electrolyte (higher concentration of carbon additive). Indeed, the high coulombic efficiencies of >99% and utilization rates for the active material of 157 mAh $g_{MnO_2}^{-1}$ (estimated as 0.2 g_{MnO_2}/mL_{SSE} * 0.5 mL_{cavity} = 0.1 g_{MnO_2} in the cell) indicates that this formulation is a good candidate for the demonstration of the battery concept. In terms of cyclability, the different utilization rate of MnO_2 for the three batteries led to different areal capacities and operating time for similar number of cycles. As a result, cyclability of the three batteries cannot be easily compared. For instance, areal capacity and operating time for Mn45Zn60 is 3-time larger than that of Mn60Zn60 so that Zn electrode is much more stressed for Mn45Zn60 (utilization and corrosion). Indeed, the lower utilization rate of MnO_2 for Mn60Zn60 leads to a buffer of Zn (two third of the Zn is not used). On the most demanding conditions (battery Mn45Zn60), a capacity retention of 70% after 50 cycles and 144 h of operation is obtained, which is attributed to the spontaneous corrosion of Zn and consequently evolution of the pH [18,19]. Likely, corrosion is enhanced using Zn powder and high surface area carbon with respect to Zn foil. Different strategies proposed in the literature [20–33] can be explored in future works to improve this aspect. Preliminary results are briefly discussed in the last section of this work. Nonetheless, corrosion of Zn was mitigated by increasing its content in the Zn-SSE: since the amount of MnO_2 is the same than the Zn (2.55 mmol), an excess of Zn

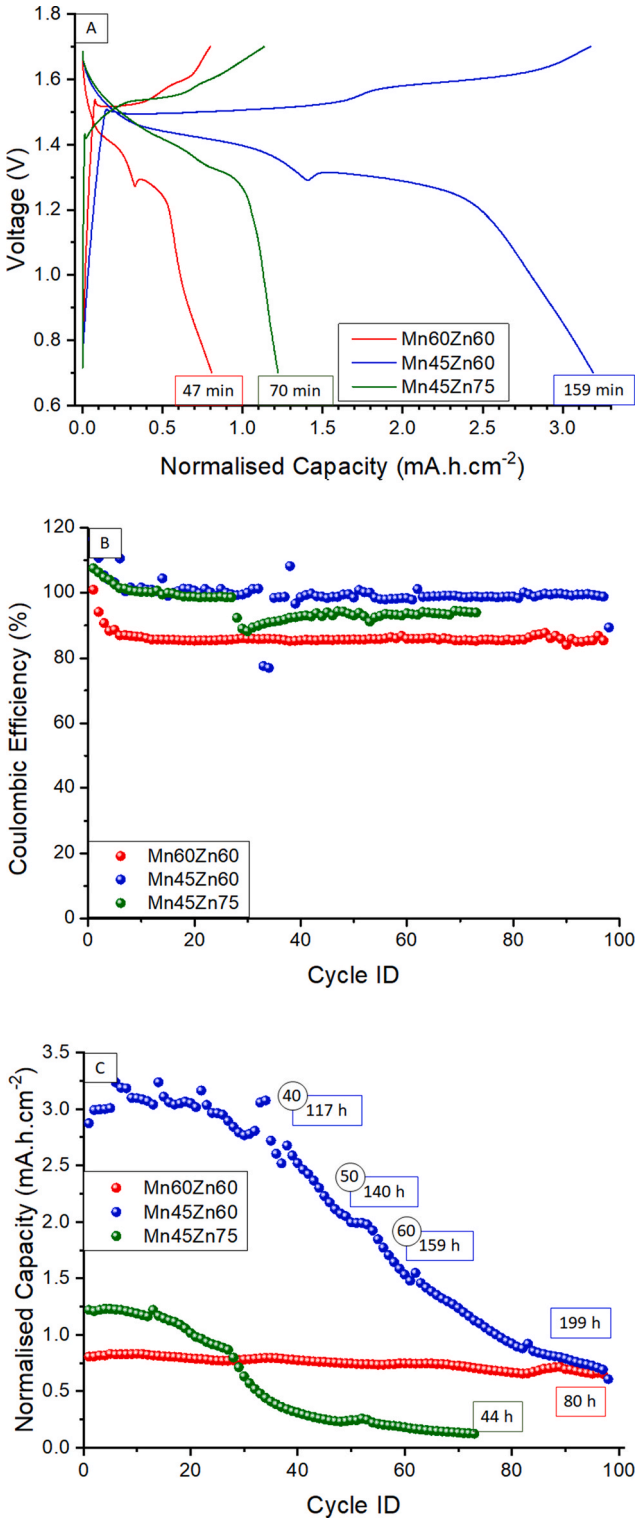

Fig. 6. (A) Voltage profiles, (B) coulombic efficiency and (C) normalised capacity for the Zn–MnO_2 injected batteries with different SSEs (1 g MnO_2 and 0.375 g carbon, 1 g Zn and 0.420 g carbon dispersed in different electrolyte volumes).

was added (2 g instead of 1 g) to compensate the spontaneous Zn corrosion, observing an increase in the normalised capacity up to 4.71 $mAh.cm^{-2}$ for the first cycle (Fig. S3), increasing the utilization rate to the theoretical value (231 mAh $g_{MnO_2}^{-1}$) and the cycle stability (retention of 85% after 189 h of operation). Due to the relatively high porosity of

this SSE, the specific capacity considering MnO_2 + carbon + electrolyte (151 Ah $g^{-1}_{total\ cathode}$) needs to be improved in future works.

3.5. Electrochemical characterisation of complex-shape batteries

The logo of our university (University of Burgos-UBU) was used as case study to demonstrate the proof-of-concept for the fabrication of complex-shape batteries using the proposed approach. Drawings of the battery cell are displayed in Fig. S4. The thickness of the cavities for the SSEs is 1 mm. For such design and manual injection, only SSEs with a shear thinning and thixotropic behaviour could be easily injected into this complex-shape cell, which was anticipated by the injection tests shown in Fig. 4, where those thixotropic SSEs could be used for injecting any shape while SSEs exhibiting anti-thixotropic (rheopectic) behaviour were suitable only for simple geometries with relatively short lengths. Thus, a battery was prepared using Zn and MnO_2 SSEs with 6.0 mL of electrolyte. The battery was successfully fabricated, and the electrochemical performances are shown in Fig. 7. The results obtained for this UBU-shape battery are comparable with those recorded for simple-shape using the same formulations for the SSEs (Fig. 6). This means that while cycle stability was good, the areal capacity was low. Indeed, the voltage profile of Zn–MnO_2 showed the typical bump at 50% depth of discharge during discharge process. The evolution of the voltage at which this characteristic voltage bump takes place upon cycling did not change significantly (0.4 mV h^{-1} over 50 h, Fig. S5), which indicates that internal resistance did not evolve significantly over time and confirming the lack of major sedimentation. Obviously, the best performing SSEs (Mn45Zn60) using an excess of Zn was the best option for the UBU-shape battery, but it could not be injected due to their rheological properties. Nevertheless, the versatility of additive manufacturing enables the modification of cell design to inject successfully anti-thixotropic SSEs that showed the best electrochemical performances. Among multiple options, two modifications were introduced. First, a second inlet was added at the end of the SSE cavity, where the outlet was originally located. Consequently, the outlets for the SSEs were moved into the half of the cell. Despite this modification facilitated the injection by achieving a filling of the 80% of the cell in the best cases, the anti-thixotropic behaviour was too strong to allow full injection of the cell. A second modification was introduced in the original design: an increase of the cavity thickness to increase the section through which the SSE flows (Fig. S6). After introducing these two modifications, the battery was injected without problems despite its anti-thixotropic behaviour (Mn45Zn60). The voltage profiles of the resulting UBU-shaped battery are shown in Fig. S7A, which are consistent with the previous results. A 6 folds increase in areal capacity from 0.7 $mAhcm^{-2}$ (1 mm thick, Fig. 7) to 4.5 $mAhcm^{-2}$ (2 mm thick, Fig. S7) was obtained when the thickness was increased by two folds, indicating a better electrochemical performance of the anti-thixotropic SSEs. Interestingly, the coulombic efficiency decreased to 80% (Fig. S7B). Probably the high thickness of 2 mm together with the high surface area of SSEs led to increase electrolyte decomposition at both electrodes. Thus, changes in the cell design affect battery performance, so that proper optimization should be conducted for optimal performances.

Finally, the new approach for the fabrication of shape-conformable batteries proposed in this work should be valid for other battery chemistries. Among the various options, aqueous Prussian blue and Zn–$LiFePO_4$ in super-concentrated electrolyte (water-in-salt) were chosen since these systems have been reported to deliver improved cycle stabilities [34–38]. Preliminary results using other battery chemistries confirmed the versatility of the concept (Fig. S8). Indeed, capacity retention was improved with respect to Zn–MnO_2 indicating that spontaneous oxidation of Zn accelerated in powder form is likely responsible for the relatively fast capacity decay observed in the previous results.

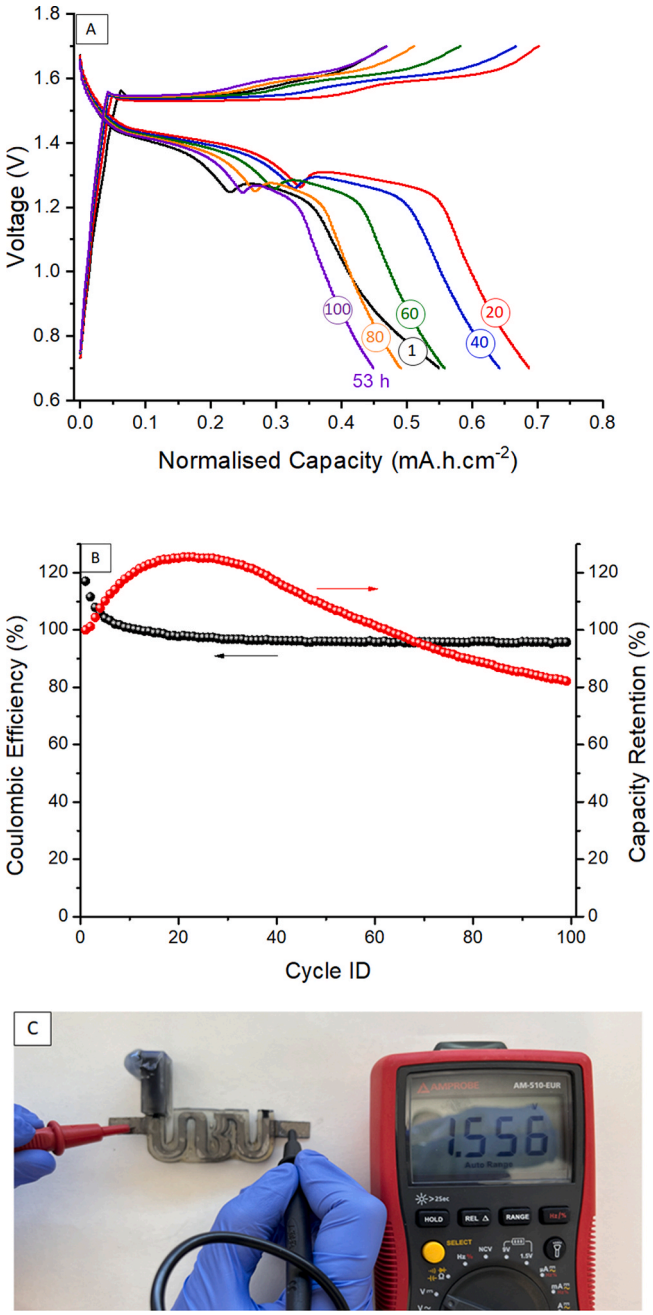

Fig. 7. (A) Voltage-capacity profiles for different cycles of the UBU shape battery (1 mm thick) filled with 1 g MnO_2 and 0.375 g carbon, 2 g Zn and 0.420 g carbon SSEs using 6.0 mL of electrolyte, (B) coulombic efficiency and capacity retention and (C) optical picture immediately after injection of SSEs (still with the connectors in the upper left corner).

4. Conclusions

This work demonstrates a new fabrication process for shape-conformable batteries based on the fabrication of complex-shape cells using additive manufacturing (AM) followed by subsequent filling of the cell using semi-solid electrodes (SSEs). Several aspects are identified to be critical for the development of the proposed concept: I) the injection system, II) the rheological behaviour of the SSEs, III) the electrochemical properties of the SSEs, and IV) the geometry of the cell to be injected. After investigating these aspects using simple-shape cells, a battery having the shape of the University of Burgos logo (UBU) is used as case study for the demonstration of the proposed approach. While anti-

thixotropy viscosity curves hinder proper filling of the SSE in complex-shape cells, SSEs with thixotropic behaviour facilitates injection. Moreover, the flexibility of AM enables slight changes in the cell design so that even SSE having anti-thixotropy behaviour could be used. The prototype having the shape of "UBU" delivers comparable performances than those obtained for simple-shape cells, while the intrinsic characteristics of Zn–MnO_2, specifically the spontaneous corrosion of Zn powder, limits the cycle stability. Indeed, improved cycle stability results are obtained when the proposed approach is implemented for other battery chemistries, e.g., aqueous Prussian blue analogues and Zn–Li-$FePO_4$ in super-concentrated aqueous electrolytes. Improving the properties of SSE through the addition of surfactants, optimization of formulations, etc., will be of key importance to reach competitive performance for the proposed battery technology.

CRediT authorship contribution statement

Mario Borlaf: Methodology, Investigation, Visualization, Writing – original draft. **Rodrigo Moreno:** Methodology, Writing – review & editing, Supervision. **Edgar Ventosa:** Conceptualization, Methodology, Writing – review & editing, Supervision, Funding acquisition.

Declaration of competing interest

The authors declare that they have no known competing financial interests or personal relationships that could have appeared to influence the work reported in this paper.

Data availability

Data will be made available on request.

Acknowledgements

The authors acknowledge the financial support by "Fundación la Caixa", under agreement LCF/PR/PR18/51130007. The authors also acknowledge the financial support by the Spanish Ministry of Science and Innovation and NextGenerationEU (TED2021-131651B–C21) and Ramón y Cajal award (Ministry of Science and Innovation and European Social Funds, RYC2018-026086-I). This work was supported by the Regional Government of Castilla y León (Junta de Castilla y León) and by the Ministry of Science and Innovation MICIN and the European Union NextGenerationEU/PRTR.

Appendix A. Supplementary data

Supplementary data to this article can be found online at https://doi.org/10.1016/j.jpowsour.2023.233063.

References

[1] A. Maurel, A.C. Martinez, S. Grugeon, S. Panier, L. Dupont, P. Cortes, C. G. Sherrard, I. Small, S.T. Sreenivasan, E. MacDonald, Toward high resolution 3D printing of shape-conformable batteries via vat photopolymerization: review and perspective, IEEE Access 9 (2021) 140654–140666, https://doi.org/10.1109/ACCESS.2021.3119533.

[2] H. Ragones, S. Menkin, Y. Kamir, A. Gladkikh, T. Mukra, G. Kosa, D. Golodnitsky, Towards smart free form-factor 3D printable batteries, Sustain. Energy Fuels 2 (2018) 1542–1549, https://doi.org/10.1039/C8SE00122G.

[3] L.E. Asp, K. Bouton, D. Carlstedt, S. Duan, R. Harnden, W. Johannisson, M. Johansen, M.K.G. Johansson, G. Lindbergh, F. Liu, K. Peuvot, L.M. Schneider, J. Xu, D. Zenkert, A structural battery and its multifunctional performance, Advanced Energy and Sustainability Research 2 (2021), 2000093, https://doi.org/10.1002/AESR.202000093.

[4] A. Maurel, S. Grugeon, M. Armand, B. Fleutot, M. Courty, K. Prashantha, C. Davoisne, H. Tortajada, S. Panier, L. Dupont, Overview on lithium-ion battery 3D-printing by means of material extrusion, ECS Trans. 98 (2020) 3–21, https://doi.org/10.1149/09813.0003ECST/XML.

[5] S.H. Kim, K.H. Choi, S.J. Cho, S. Choi, S. Park, S.Y. Lee, Printable solid-state lithium-ion batteries: a new route toward shape-conformable power sources with aesthetic versatility for flexible electronics, Nano Lett. 15 (2015) 5168–5177, https://doi.org/10.1021/ACS.NANOLETT.5B01394/SUPPL_FILE/NL5B01394_SI_001.PDF.

[6] Y. Yang, W. Yuan, X. Zhang, Y. Yuan, C. Wang, Y. Ye, Y. Huang, Z. Qiu, Y. Tang, Overview on the applications of three-dimensional printing for rechargeable lithium-ion batteries, Appl. Energy 257 (2020), 114002, https://doi.org/10.1016/j.apenergy.2019.114002.

[7] Y. Pang, Y. Cao, Y. Chu, M. Liu, K. Snyder, D. MacKenzie, C. Cao, Additive manufacturing of batteries, Adv. Funct. Mater. 30 (2020), 1906244, https://doi.org/10.1002/adfm.201906244.

[8] M. Duduta, B. Ho, V.C. Wood, P. Limthongkul, V.E. Brunini, W.C. Carter, Y. Chiang, M. Duduta, B. Ho, V.C. Wood, P. Limthongkul, V.E. Brunini, W. Craig Carter, Y.-M. Chiang, Semi-solid lithium rechargeable flow battery, Adv. Energy Mater. 1 (2011) 511–516, https://doi.org/10.1002/AENM.201100152.

[9] Z. Li, K.C. Smith, Y. Dong, N. Baram, F.Y. Fan, J. Xie, P. Limthongkul, W.C. Carter, Y.M. Chiang, Aqueous semi-solid flow cell: demonstration and analysis, Phys. Chem. Chem. Phys. 15 (2013) 15833–15839, https://doi.org/10.1039/C3CP53428F.

[10] F.Y. Fan, W.H. Woodford, Z. Li, N. Baram, K.C. Smith, A. Helal, G.H. McKinley, W. C. Carter, Y.M. Chiang, Polysulfide flow batteries enabled by percolating nanoscale conductor networks, Nano Lett. 14 (2014) 2210–2218, https://doi.org/10.1021/NL500740T/SUPPL_FILE/NL500740T_SI_003.MOV.

[11] E. Ventosa, D. Buchholz, S. Klink, C. Flox, L.G. Chagas, C. Vaalma, W. Schuhmann, S. Passerini, J.R. Morante, Non-aqueous semi-solid flow battery based on Na-ion chemistry. P2-type $Na_xNi_{0.22}Co_{0.11}Mn_{0.66}O_2$–$NaTi_2(PO_4)_3$, Chem. Commun. 51 (2015) 7298–7301, https://doi.org/10.1039/C4CC09597A.

[12] D. Muñoz-Torrero, J. Palma, R. Marcilla, E. Ventosa, Al-ion battery based on semisolid electrodes for higher specific energy and lower cost, ACS Appl. Energy Mater. 3 (2020) 2285–2289, https://doi.org/10.1021/ACSAEM.9B02253/ASSET/IMAGES/LARGE/AE9B02253_0005.JPEG.

[13] D. Perez-Antolin, R. Trócoli, J. Palma, E. Ventosa, The injectable battery. A conceptually new strategy in pursue of a sustainable and circular battery model, J. Power Sources 480 (2020), 228839, https://doi.org/10.1016/J.JPOWSOUR.2020.228839.

[14] D. Perez-Antolin, W. Schuhmann, J. Palma, E. Ventosa, Semi-flowable Zn semi-solid electrodes as renewable energy carrier for refillable Zn–Air batteries, J. Power Sources 536 (2022), 231480, https://doi.org/10.1016/J.JPOWSOUR.2022.231480.

[15] D. Perez-Antolin, C. Irastorza, S. Gonzalez, R. Moreno, E. García-Quismondo, J. Palma, J.J. Lado, E. Ventosa, Regenerative electrochemical ion pumping cell based on semi-solid electrodes for sustainable Li recovery, Desalination 533 (2022), 115764, https://doi.org/10.1016/J.DESAL.2022.115764.

[16] B. Akuzum, P. Singh, D.A. Eichfeld, L. Agartan, S. Uzun, Y. Gogotsi, E. Caglan Kumbur, Percolation characteristics of conductive additives for capacitive flowable (Semi-Solid) electrodes, Appl. Mater. Interfaces. 12 (2020) 5875, https://doi.org/10.1021/acsami.9b19739.

[17] M. Winter, R.J. Brodd, What are batteries, fuel cells, and supercapacitors? Chem. Rev. 104 (2004) 4245–4269, https://doi.org/10.1021/cr020730k.

[18] D. Perez-Antolin, I. Sáez-Bernal, A. Colina, E. Ventosa, Float-charging protocol in rechargeable Zn–MnO_2 batteries: unraveling the key role of Mn^{2+} additives in preventing spontaneous pH changes, Electrochem. Commun. 138 (2022), 107271, https://doi.org/10.1016/J.ELECOM.2022.107271.

[19] J. Yang, J. Cao, Y. Peng, W. Yang, S. Barg, Z. Liu, I.A. Kinloch, M.A. Bissett, R.A. W. Dryfe, Unravelling the mechanism of rechargeable aqueous Zn–MnO_2 batteries: implementation of charging process by electrodeposition of MnO_2, ChemSusChem 13 (2020) 4103–4110, https://doi.org/10.1002/CSSC.202001216.

[20] A. Bayaguud, X. Luo, Y. Fu, C. Zhu, Cationic surfactant-type electrolyte additive enables three-dimensional dendrite-free zinc anode for stable zinc-ion batteries, ACS Energy Lett. 5 (2020) 3012–3020, https://doi.org/10.1021/acsenergylett.0c01792.

[21] R.K. Ghavami, Z. Rafiei, S.M. Tabatabaei, Effects of cationic CTAB and anionic SDBS surfactants on the performance of Zn-MnO_2 alkaline batteries, J. Power Sources 164 (2007) 934–946, https://doi.org/10.1016/j.jpowsour.2006.10.084.

[22] M. Chamoun, W.R. Brant, C.W. Tai, G. Karlsson, D. Noréus, Rechargeability of aqueous sulfate Zn/MnO_2 batteries enhanced by accessible Mn^{2+} ions, Energy Storage Mater. 15 (2018) 351–360, https://doi.org/10.1016/j.ensm.2018.06.019.

[23] S. Chen, R. Lan, J. Humphreys, S. Tao, Salt-concentrated acetate electrolytes for a high voltage aqueous Zn/MnO_2 battery, Energy Storage Mater. 28 (2020) 205–215, https://doi.org/10.1016/j.ensm.2020.03.011.

[24] C. Qiu, X. Zhu, L. Xue, M. Ni, Y. Zhao, B. Liu, H. Xia, The function of Mn^{2+} additive in aqueous electrolyte for Zn/δ-MnO_2 battery, Electrochim. Acta 351 (2020), 136445, https://doi.org/10.1016/j.electacta.2020.136445.

[25] M. Minakshi, P. Singh, M. Carter, K. Prince, The Zn-MnO_2 battery: the influence of aqueous LiOH and KOH electrolytes on the intercalation mechanism, Electrochem. Solid State Lett. 11 (2008) A145, https://doi.org/10.1149/1.2932056.

[26] X. Zeng, J. Liu, J. Mao, J. Hao, Z. Wang, S. Zhou, C.D. Ling, Z. Guo, Toward a reversible Mn^{4+}/Mn^{2+} redox reaction and dendrite-free Zn anode in near-neutral aqueous Zn/MnO_2 batteries via salt anion chemistry, Adv. Energy Mater. 10 (2020), 1904163, https://doi.org/10.1002/aenm.201904163.

[27] C. Xie, T. Li, C. Deng, Y. Song, H. Zhang, X. Li, A highly reversible neutral zinc/manganese battery for stationary energy storage, Energy Environ. Sci. 13 (2020) 135–143, https://doi.org/10.1039/c9ee03702k.

[28] G.G. Yadav, D. Turney, J. Huang, X. Wei, S. Banerjee, Breaking the 2 v barrier in aqueous zinc chemistry: creating 2.45 and 2.8 v MnO_2-Zn aqueous batteries, ACS Energy Lett. 4 (2019) 2144–2146, https://doi.org/10.1021/acsenergylett.9b01643.

[29] J. Hao, X. Li, S. Zhang, F. Yang, X. Zeng, S. Zhang, G. Bo, C. Wang, Z. Guo, Designing dendrite-free zinc anodes for advanced aqueous zinc batteries, Adv. Funct. Mater. 30 (2020), 2001263, https://doi.org/10.1002/adfm.202001263.
[30] S.A. Mehta, A. Bonakdarpour, D.P. Wilkinson, Impact of cathode additives on the cycling performance of rechargeable alkaline manganese dioxide–zinc batteries for energy storage applications, J. Appl. Electrochem. 47 (2017) 167–181, https://doi.org/10.1007/s10800-016-1034-1.
[31] M. Kelly, J. Duay, T.N. Lambert, R. Aidun, Impact of triethanolamine as an additive for rechargeable alkaline Zn/MnO_2 batteries under limited depth of discharge conditions, J. Electrochem. Soc. 164 (2017) A3684–A3691, https://doi.org/10.1149/2.0641714jes.
[32] J.P. Tafur, J. Abad, E. Román, A.J. Fernández Romero, Charge storage mechanism of MnO_2 cathodes in Zn/MnO_2 batteries using ionic liquid-based gel polymer electrolytes, Electrochem. Commun. 60 (2015) 190–194, https://doi.org/10.1016/j.elecom.2015.09.011.
[33] B.J. Hertzberg, A. Huang, A. Hsieh, M. Chamoun, G. Davies, J.K. Seo, Z. Zhong, M. Croft, C. Erdonmez, Y.S. Meng, D. Steingart, Effect of multiple cation electrolyte mixtures on rechargeable Zn-MnO_2 alkaline battery, Chem. Mater. 28 (2016) 4536–4545, https://doi.org/10.1021/acs.chemmater.6b00232.
[34] J. Qian, C. Wu, Y. Cao, Z. Ma, Y. Huang, X. Ai, H. Yang, Prussian blue cathode materials for sodium-ion batteries and other ion batteries, Adv. Energy Mater. 8 (2018), 1702619, https://doi.org/10.1002/AENM.201702619.
[35] J. Hao, J. Long, B. Li, X. Li, S. Zhang, F. Yang, X. Zeng, Z. Yang, W. Kong Pang, Z. Guo, J. Hao, J. Long, X. Li, S. Zhang, F. Yang, X. Zeng, W.K. Pang, Z. Guo, Z. Yang, B. Li, Toward high-performance hybrid Zn-based batteries via deeply understanding their mechanism and using electrolyte additive, Adv. Funct. Mater. 29 (2019), 1903605, https://doi.org/10.1002/ADFM.201903605.
[36] M. Pasta, C.D. Wessells, R.A. Huggins, Y. Cui, A high-rate and long cycle life aqueous electrolyte battery for grid-scale energy storage, Nat. Commun. 1 (3) (2012) 1–7, https://doi.org/10.1038/ncomms2139, 2012 3.
[37] H.W. Lee, R.Y. Wang, M. Pasta, S.W. Lee, N. Liu, Y. Cui, Manganese hexacyanomanganate open framework as a high-capacity positive electrode material for sodium-ion batteries, Nat. Commun. 1 (5) (2014) 1–6, https://doi.org/10.1038/ncomms6280, 2014 5.
[38] L. Ma, M.A. Schroeder, O. Borodin, T.P. Pollard, M.S. Ding, C. Wang, K. Xu, Realizing high zinc reversibility in rechargeable batteries, Nat. Energy 10 (5) (2020) 743–749, https://doi.org/10.1038/s41560-020-0674-x, 2020 5.